BNL-211987-2019-JAAM

Revealing the Effects of Trace Oxygen Vacancies on Improper Ferroelectric Manganite with In Situ Biasing

S. Cheng

To be published in "ADVANCED ELECTRONIC MATERIALS"

April 2019

Condensed Matter Physics and Materials Science Department

Brookhaven National Laboratory

U.S. Department of Energy

USDOE Office of Science (SC), Basic Energy Sciences (BES) (SC-22)

DISCLAIMER

DOI: 10.1002/((please add manuscript number))
Article type: Full paper

Revealing the effects of trace oxygen vacancies on improper ferroelectric manganite with *in-situ* biasing

Shaobo Cheng, Qingping Meng, Myung-Geun Han, Shiqing Deng, Xing Li, Qinghua Zhang, Guotai Tan, Gianluigi A. Botton, Yimei Zhu**

Prof. Yimei Zhu, Dr. Shaobo Cheng, Dr. Qingping Meng, Dr. Myung-Geun Han
Condensed Matter Physics and Materials Science, Brookhaven National Laboratory, Upton, NY 11973, USA
*E-mail: zhu@bnl.gov
chengs36@mcmaster.ca

Prof. Gianluigi A. Botton, Dr. Shaobo Cheng
Department of Materials Science and Engineering, McMaster University, Hamilton, Ontario, L8S 4L7, Canada

Mr. Shiqing Deng
School of Materials Science and Engineering, Tsinghua University, Beijing 100084, China

Dr. Xing Li
Key Laboratory of Materials Physics of Ministry of Education, Department of Physics and Engineering, Zhengzhou University, Zhengzhou 450052, China

Dr. Qinghua Zhang
Beijing National Laboratory for Condensed Matter Physics Institute of Physics, Chinese Academy of Sciences, Beijing 100190, China

Prof. Guotai Tan
Department of Physics, Beijing Normal University, Beijing 100875, China

Keywords: *in-situ* biasing, domain switching, hexagonal manganites, oxygen vacancies

Abstract

Multiferroic materials, which exhibit multiple orderings, are promising for next generation data-storage device applications. $YMnO_3$, in particular, because of the coexistence of the ferroelectricity and (anti)ferromagnetism within one single material, has drawn special attentions to application-based research. However, the role of defect chemistry related to the behaviors of the ferroelectric polarization has been seldomly studied due to its complexity. In

this work, we report a novel switching behavior of multiferroic $YMnO_3$ single crystal using *in-situ* biasing and Landau based numerical calculation. We reveal that the domain switching only happens at the topmost surface, which can be well explained by the electric field redistribution due to the trace amount of oxygen vacancies. Our *in-situ* observations demonstrate that defect chemistry plays an important role in domain switching and can be utilized as an additional parameter for controlling the distribution of electric field within the multiferroic materials.

Main Text

Multiferroic materials possess a wide range of properties that make them attractive for versatile microelectronic applications.[1,2] Hexagonal manganites is a big family of single phase multiferroic materials, where multiple orderings coexist within one single material. The successful application of single phase multiferroic materials would dramatically reduce the difficulties for the device fabrication. The domains of hexagonal manganites remain stable under continuous deformation or perturbation due to the existence of topologically protected properties.[3] Different types of topological defects have been found in hexagonal rare-earth manganites and they have strong interactions between each other.[4-7] $YMnO_3$, as a prototypical hexagonal manganite, exhibits improper ferroelectricity ($T_C \approx 1000K$) and geometric frustrated (anti)ferromagnetism ($T_N \approx 70K$).[8-11] The hexagonal cell of $YMnO_3$ with downward polarization direction is shown in **Figure 1(a)**. Because of its hexagonal symmetry (space group: $P6_3cm$), $YMnO_3$ has uniaxial anisotropy and two ferroelectric polarization directions. The order parameter space for $YMnO_3$ is composed of six order parameters ($\alpha+$, $\alpha-$, $\beta+$, $\beta-$, $\gamma+$, $\gamma-$): three types of antiphases (α, β, and γ) and each type is accompanied with two kinds of polarization directions ("+" being parallel with *c*-axis, while "-" being antiparallel with *c*-axis). The ferroelectric domain walls are always coupled with the antiferromagnetic

domain walls, thus the manipulation of the electric domains is equivalent to the manipulation of the magnetic domains, making this system even more interesting.[11]

Although the defect chemistry is one of the most ineluctable obstacles to the reliability and functionality of multiferroic devices, there are few studies reported. The previous experimental results indicate that the sample fabrication process (in air or in Ar) would affect the domain structures and even the physical properties of $YMnO_3$, making them attractive system to study the defect chemistry.[12-14] The $YMnO_3$ single crystals used in this work were fabricated by floating zone method in Ar atmosphere.[15] The orthorhombic phase $YMnO_3$ can be realized when it was grown on certain kinds of substrates and the ferroelectric transition temperature is about 40K, which is not suitable for room temperature transmission electron microscopy (TEM) studies.[16] Ferroelectric materials are conventionally regarded as insulators with a constant permittivity through the whole samples. In reality, the oxygen vacancies in ferroelectric materials can strongly affect their conductivity. Theoretical considerations suggest that the concentration of oxygen vacancies can significantly alter the distribution of electric potential in ferroelectric materials as well.[17]

The polarization stability and domain flipping in multiferroic materials are very important for future device applications, but the functional properties of point defect in domain dynamics remain unclear. *In-situ* biasing in TEM would be a great benefit for this type of studies and it has been broadly used for studying the domain switching behaviors. Han, *et al* have revealed that the vortex core in hexagonal manganites won't change under external biasing.[5] Gao, *et al* have found that the dislocations (line defect) have pinning effects on the movement of domains.[18] The synthesized $YMnO_3$ samples were unable to measure the ferroelectric hysteresis loop. Here, we study ferroelectric switching using *in-situ* biasing in TEM, and the effects of trace oxygen vacancies on the domain switching behaviors are demonstrated.

Since $YMnO_3$ has strong uniaxial anisotropy, we tried to apply an electric field with constant voltage along *c*-axis. We did not apply pulsed voltage due to the significant back switching in this case (there would be no change in domain structure before and after a voltage pulse). The low magnificaiton scanning electron microscopy (SEM) image for the focused ion beam (FIB) sample is shown in Figure 1(b). The sample was laid atop of Mo grid. The corresponding selected area electron diffraction (SAED) pattern is embedded, showing the orientation of the sample. The observation is along [100], which is most suitable direction for observing the ferroelectric domains. **Figure 2(a)** is the low magnification TEM image. The movable tungsten tip was in contact with the top surface of $YMnO_3$ FIB sample, which is a typical experimental configuration for *in-situ* TEM studies.[18,19] The electric field was applied between the tungstan tip and the Mo grid. The W tip was grounded as illustrated in Figure 2(b). Basic characterizations on the sample were carried out before the *in-situ* experiments. As shown in Figure 2(c), under two-beam condition, the polarization direction of each domain can be identified.[20] A six-fold vortex core (indicated by red circle) can be observed and used as the reference spot. Here, we define the "-" as the polarization direction pointing toward the surface of the sample.

In-situ TEM biasing has been extensively used for studying the dynamic behaviors of materials under different external stimuli.[7,21] In our experiments, up to 180 kV cm^{-1} electric field was applied. Figure 2(e) shows the domain configuration after 180 kV cm^{-1} biasing experiment. Interestingly, the domain switching behavior is different from what has been reported before and a novel domain switching behavior is identified.[7] The domain switching is restricted to the surface part of the sample, forming a straight domain wall front that is parallel to the surface of the FIB sample. The domain switching happens immediately after the electric field was applied. It is worthwhile to mention that the domains expand faster along the direction that is parallel to the surface compared with that along the depth direction. However, the shapes of domains inside of the sample remain the same. The slight variation of

relative domain contrast in TEM images is caused by the different positions of the objective aperture.[20] High resolution high-angle annular dark-field scanning transmission electron microscopy (HAADF-STEM) images have been taken to identify the ferroelectric polarization direction and the phase of each domain. The corresponding high resolution images for the small white dashed rectangle areas (h, g, i) in Figure 2(e) can be found in Figure 2(g)-(i), respectively. The atomic models are also embeded in Figure 2(g) and the domain walls are highlighted by red lines. Figure 2(d) and (f) are the schematic diagrams with better domain contrast for the Figure 2(c) and (e), respectively.

In our *in-situ* experiments, different electric fields (30 kV cm^{-1} to 180 kV cm^{-1}) have been applied to the sample. In **Figure 3(a)**, 60 kV cm^{-1} external biasing was applied and the domain switching occurred at the topmost surface. After removing the bias, the domain retention behavior can be observed (Figure 3(b)). The switched domain can be erased after an inverse electric field (-60 kV cm^{-1}) being applied (as indicated in Figure 3(c)). Furthermore, a series of biasing experiments were carried out, denoted in an alphabetical order, and correspondingly illustrated in **Figure 4(a) -(c), (g), (h)**. With the increasing biasing from 30 kV cm^{-1} to 180 kV cm^{-1}, it is found that the applied electric field can make the domains expand if the polarization direction is parallel to the electric field and make them shrink for the opposite case, which is a typical phenomenon in the ferroelectric domain switching. Since $YMnO_3$ has the topologically protected domains, the ferroelectric domain with certain phase (α, β, or γ) will never be eliminated. The width between the domain switching front and the sample surface (denoted by "w" in Figure 4) increases with the stronger external electric field. A linear-like relationship between the width of domains and the field strength is plotted in Figure 4(i). The switched domains can be maintained unless the reversed external bias has been applied. The six-fold vortex core in each figure is a position reference. No matter how strong the applied electric field was, no change was observed near the six-fold vortex core. More TEM images taken under different bias can be found in the Supporting Information.

From the EELS line scan results, no evident feature has been detected for the oxygen vacancies. Thus, the oxygen vacancies should be in small amount and uniformly distributed within $YMnO_3$ single crystalline samples. The theoretical model proposed by Zhang, *et al.* [17] indicated that the distributions of electric field in ferroelectric samples are significantly affected by the concentration of oxygen vacancies. Here, a similar model was applied to numerically examine the effects of concentration of oxygen vacancies on $YMnO_3$ single crystalline sample. The parameters of $YMnO_3$ for Landau theory calculations can be found in Ref. [22]. The details of the calculations can be found in the Supporting Information. The numerical results show that the distribution of electric field is sensitive to the concentration of oxygen vacancies, the thickness of specimen, and the applied electric fields. In our experiment, the width of FIB sample was 4 μm and the applied external electric field strength varied from 30 kV cm^{-1} to 180 kV cm^{-1}. First of all, the field strength was fixed at 90 kV cm^{-1} to investigate the effect of the carriers concentration by the calculations. The density of the carriers is twice as large as the density of oxygen vacancies (one oxygen vacancy creates two electrons), and the detailed discussion can be found in the Supporting Information. **Figure 5(a)** shows respectively the distribution of electric field strength (solid lines) and of electric potential (dashed lines). The distribution of electric field strength sensitively depends on the concentration of oxygen vacancies in specimen. The width of the sample is defined in Figure 2(b). The zero position for the *x*-axis is the top surface of the sample. When the density of charge carriers is zero (no oxygen vacancy), the electric potential drops linearly with increasing distance away from the sample surface and so the strength of field remains constant across the whole sample. In this case, the domain switching will happen across whole sample if the bias is applied. However, the existence of oxygen vacancies will change the distribution of electric field in ferroelectric materials, and the redistributed electric field would result in the different behaviors of domain switching. For the low concentration case

(carrier density of 10^{21} m^{-3}), as represented by the black lines in Figure 5 (a), the electric potential is no longer linear (black dashed line) so that the electric field strength gradually decreases away from the surface. For the sample with higher concentration of charge carriers (10^{23} m^{-3} and 10^{24} m^{-3}), the electric potential and electric field strength deplete faster when it is away from surface. The pink and blue circles mark the inflection points of the electric fields, where the slopes of curves promptly change to zero from finite values. The electric field is relative strong for the area below the inflection point. Because of the depletion region of the electric field, the domain switching along width direction is depressed. According to our theoretical results published elsewhere, the velocity of domain expansion sensitively depends on the electric field strength in samples.[23] The higher the electric field strength, the faster the domains expand. The non-uniform distribution of the electric field in the sample results in the fact that the electric field strength quickly decreases from the topmost surface to internal. The domain expansion prefers to grow along surface direction rather than the depth direction, which also fits well with our experimental observation. The inflection point will shift more to zero point of *x*-axis with higher charge carriers concentration and lower electric field strength. Figure 5(b) shows the relationship between the positions of the inflection points and the applied electric field strength with the carrier densities of 10^{23} and 10^{24} m^{-3}. The positions of the inflection points have linear-like correlation with increasing the applied electric field. The positions of the inflection points should correspond to the width of switched domains. The experimental result in Figure 4(i) is replotted in Figure 5(b), and we can infer that the charge carriers concentration of our sample is between 10^{23} m^{-3} and 10^{24} m^{-3}. The charge carrier concentration of 10^{23} m^{-3} indicates that there are 5×10^{-6} oxygen vacancy in each chemical formula, which is not possible to be detected in our experiments.

As a matter of fact, this could also be a good method to indicate the charge carrier density within a ferroelectric sample experimentally. We could measure the widths of the switched domains under different external applied bias, and compare these values with the theoretical

widths calculated from sample models with different charge carriers densities. Thus, the charge carrier densities and the concentration of oxygen vacancies within the samples can be quantitatively evaluated.

Conclusions:

In this work, with the assistance of *in-situ* TEM techniques, we experimentally explored the influence of the defect chemistry (oxygen vacancies) on the functional properties of hexagonal multiferroic single crystalline $YMnO_3$. The sample shows a novel switching dynamic behavior: the domain switching is limited to the topmost surface region. Trace amount of oxygen vacancies were formed in the $YMnO_3$ samples due to the fabrication condition of our sample. These defects lead to a non-uniform distribution of the electric field across the sample and the thus restrict the domain switching to the surface area, which has been quantitively confirmed by our Landau based numerical calculations. This result also successfully explains the fact that the ferroelectric hysteresis loop cannot be measured on this sample, since the external electric field has only applied to the top surface. Furthermore, the domain switching behaviors can also be treated as a method for evaluating the concentration of charge carriers. Our results could help to hatch new approaches for compositional designs for the realization of high performance multiferroic devices.

Experimental Section

TEM characterizations: The *in-situ* experiments were carried out by the JEOL ARM 200CF TEM with double correctors at 200kV in Brookhaven National Laboratory. A convergent angle of 21.2 mrad and a collection angle of 67-275 mrad were used for collecting the HAADF images. Wiener filter was used for some HAADF images to reduce the noise. The *in-situ* PFM holder was made by Nanofactory company. The TEM samples used for *in-situ* studies were prepared by focused ion beam (FIB) lift-out methods. Low voltage mode has

been applied to reduce/remove the surface damage layer. The FIB model is FEI Helios dual beam system in Brookhaven National Laboratory.

Supporting Information
Supporting Information is available from the Wiley Online Library or from the author.

Acknowledgements
We acknowledge the discussions with Prof. Jing Zhu from Tsinghua University. The electronic microscopy work was carried out at Brookhaven National Laboratory and supported by the U.S. DOE Basic Energy Sciences, Materials Sciences and Engineering Division under Contract No. DESC0012704. G. A. B. and S. C. are grateful to NSERC for a Discovery Grant. X. L. is grateful to National Natural Science Foundation of China (Grant No. 11804304）

Received: ((will be filled in by the editorial staff))
Revised: ((will be filled in by the editorial staff))
Published online: ((will be filled in by the editorial staff))

References

[1] W. Eerenstein, N. D. Mathur, J. F. Scott, *Nature* **2006**, *442*, 759-765

[2] X. Li, M. Sun, X. Wei, C. Shan, Q. Chen, *Nanomaterials*, **2018**, *8*, 188

[3] T. Choi, Y. Horibe, H. T. Yi, Y. J. Choi, W. Wu, S. –W. Cheong, *Nat. Mater.* **2010**, *9*, 253-258

[4] S. –Z. Lin, X. Wang, Y. Kamiya, G. –W. Chern, F. Fan, D. Fan, B. Casas, Y. Liu, V. Kiryukhin, W. H. Zurek, C. D. Batista, S. –W. Cheong, *Nat. Phys.* **2014**, *10*, 970 -977

[5] M.-G. Han, Y. M. Zhu, L. J. Wu, T. Aoki, V. Volkov, X. Y. Wang, S. C. Chae, Y. S. Oh, S.-W. Cheong, *Adv. Mater.***2013**, *25*, 2415-2421

[6] S. Cheng, J. Li, M.-G. Han, S. Deng, G. Tan, X. Zhang, J. Zhu, Y. Zhu, *Phys. Rev. Lett.* **2017**, *118*, 145501

[7] S. C. Chae, N. Lee, Y. Horibe, M. Tanimura, S. Mori, B. Gao, S. Carr, S. –W. Cheong, *Phys. Rev. Lett.* **2012**, *108*, 167603

[8] B. B. V. Aken, T. T. M. Palstra, A. Filippetti, N. A. Spaldin, *Nat. Mater.* **2004**, *3*, 164-170

[9] S. Cheng, C. Xu, S. Deng. M. –G. Han, S. Bao, J. Ma, C. Nan, W. Duan, L. Bellaiche, Y. Zhu, J. Zhu, *Sci. Adv.* **2018**, *8*, 4298

[10] A. S. Gibbs, K. S. Knight, P. Lightfoot, *Phys. Rev. B*, **2011**, *83*, 094111

[11] M. Fiebig, Th. Lottermoser, D. Fröhlich, A. V. Goltsev. R. V. Pisarev, *Nature* **2002**, *419*, 818-820

[12] Y. Du, X. Wang, D. Chen, S. Dou, Z. Cheng, M. Higgins, G. Wallace, J. Wang, *Appl. Phys. Lett.* **2011**, *99*, 252107

[13] Y. Du, X. Wang, D. Chen, Y. Yu, W. hao, Z. Cheng, S. Dou, *Phys. Chem, Chem, Phys.* **2013**, *15*, 20010-20015

[14] S. C. Chae, Y. Horibe, D. Y. Jeong, S. Rodan, N. Lee, S. -W. Cheong, *Proc. Natl. Acad. Sci*. **2010**, *107*, 21366-21370

[15] C. Fan, Z. Y. Zhao, J. D. Song, J. C. Wu, F. B. Zhang, X. F. Sun, *J. Cryst. Growth*, **2014**, *388*, 54-60

[16] M. Nakamura, Y. Tokunaga, M. Kawasaki, Y. Tokura, *Appl. Phys. Lett.* **2011**, *98*, 082902

[17] J. Zhang, M. H. Tang, J. He, *Appl. Phys. Lett.* **2010**, *96*, 122905

[18] P. Gao, C. T. Nelson, J. R. Jokissari, S.-H. Baek, C. W. Bark, Y. Zhang, E. Wang, D. G. Schlom, C. -B. Eom, X. Pan, *Nat. Commun.* **2011**, *2*, *591*

[19] P. Gao, C. T. Nelson, J. R. Jokisaari, Y. Zhang, S. -H. Baek, C. W. Bark, E. Wang, Y. Liu, J. Li, C. -B. Eom, X. Pan, *Adv. Mater.* **2012**, *24*, 1106-1110

[20] S. Cheng, Y. G. Zhao, X. F. Sun, J. Zhu, *J. Am. Ceram. Soc.* **2014**, *97*, 3371-3373

[21] X. Li, M. Sun, C. Shan, Q. Chen, X. Wei, *Adv. Mater. Interfaces* **2018**, *5*, 1701246

[22] S. Artyukhin, K. T. Delaney, N. A. Spaldin, M. Mostovoy. *Nat. Mater.***2013**, *13*, 42-49

[23] Q. Meng, M-G Han, J. Tao, G. Xu, D. O. Welch, Y. Zhu, *Phys. Rev. B* **2015**, *91*, 054104

Figures and captions:

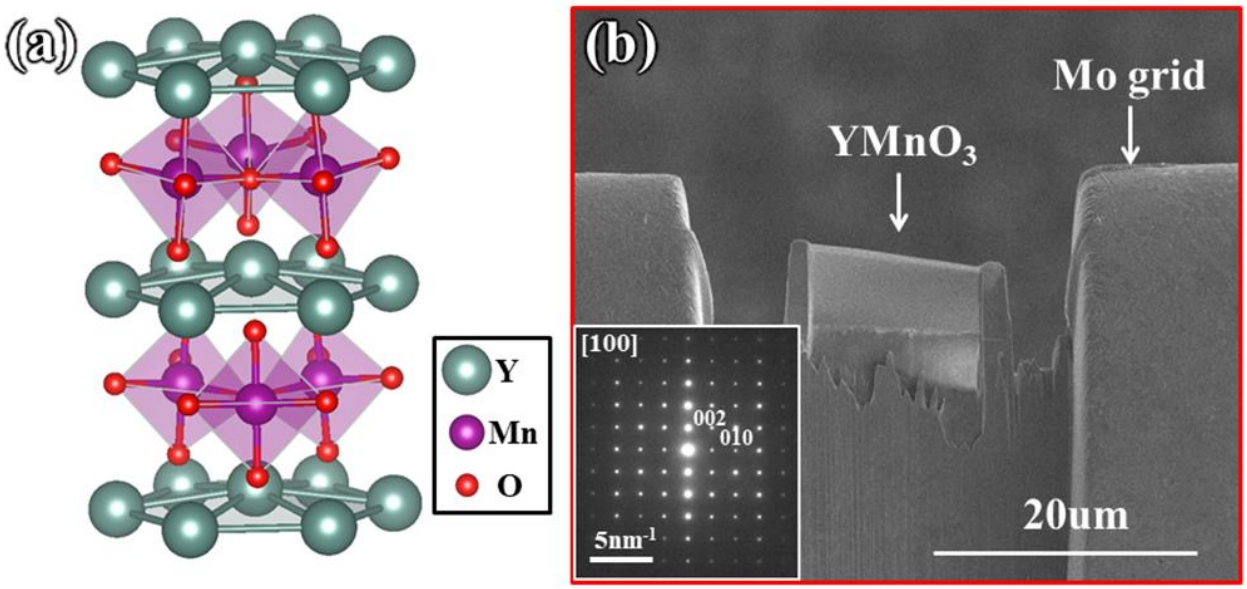

Figure 1. Atomic model and low-magnificaiton scanning electron mircoscopy (SEM) image of the $YMnO_3$. (a) Hexagonal cell of $YMnO_3$ showing its six-fold symmetry. (b) Low magnifciation SEM image showing that the FIB sample was placed on the top of Mo grid. The $YMnO_3$ sample has relative uniform thickness. Selected area electron diffraction (SAED) patterns of $YMnO_3$ is included, showing the good crystallinity of the sample and the vertically aligned *c* direction.

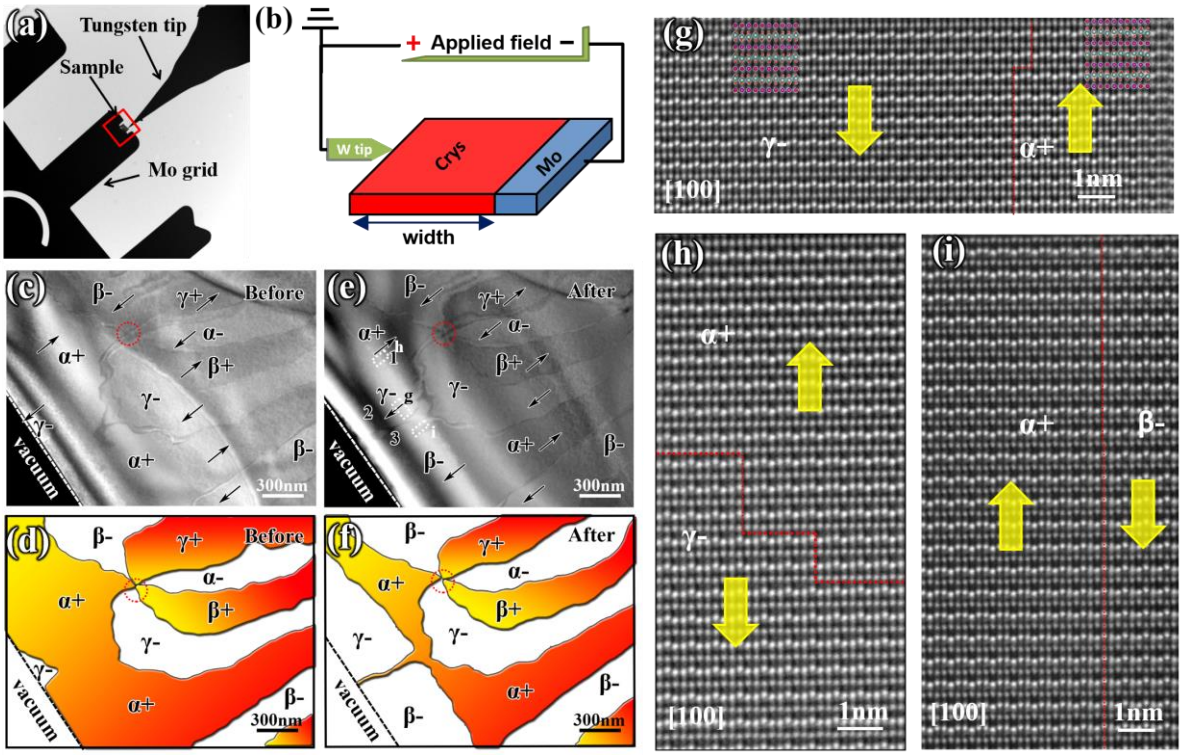

Figure 2. *In-situ* TEM experimental results and the domain configurations. (a) Low magnification TEM image showing the *in-situ* biasing experiment configuration. A movable grounded W tip makes contact with the top part of $YMnO_3$ sample. (b) Schematic diagram of the *in-situ* experiment setup. (c) The dark field TEM image showing the domain configuration at the top surface of the sample before applying electric field. A six-fold vortex core is highlighted by the red circle. (e) Dark field TEM image showing the domain configuration at the same area after 180 kV cm^{-1} biasing. The occurring of domain switching is limited to the surface areas. (d) (f) Schematic diagrams for the domain configurations in (c) and (e), respectively. (g)-(i) High resolution HAADF-STEM images for the white dashed rectangle areas in (e). The domain boundaries are highlighted by the red lines. The images are slightly filtered to reduce noise. The ferroelectric polarization directions can be indicated by the atomic configurations with up-up-down (upward polarized) or down-down-up (downward polarized).

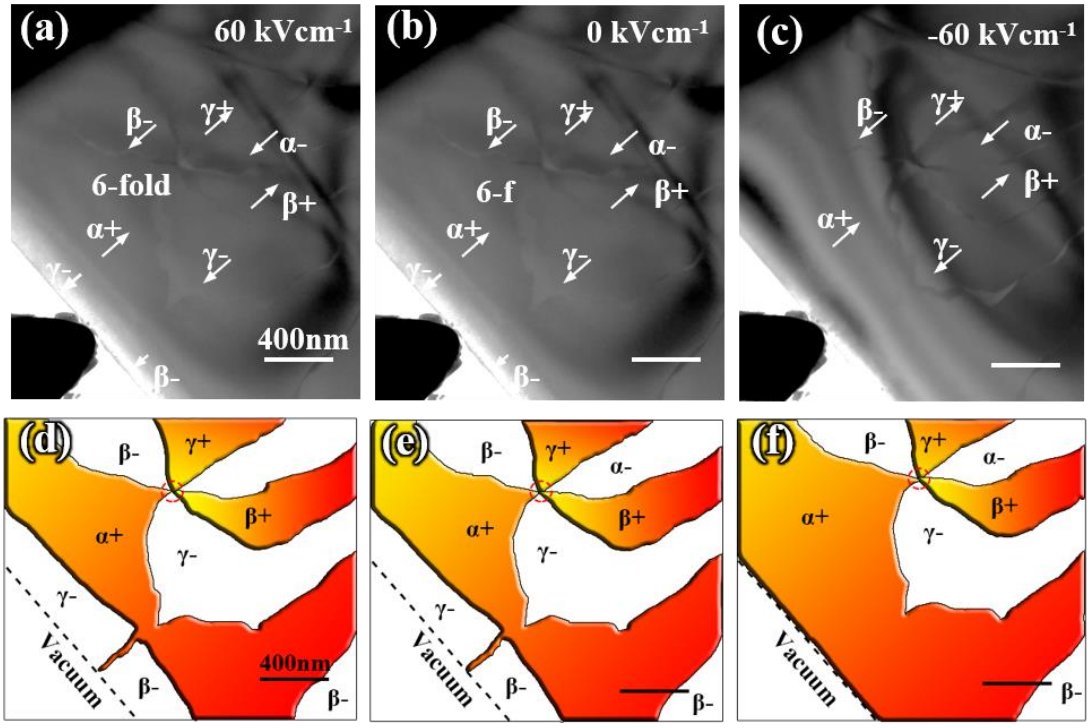

Figure 3. Writing and removal processes of the ferroelectric domains. (a) TEM image showing the domain configuration when 60 kV cm^{-1} electric field was applied to the sample. The γ- and β- domains at the surface area expand. (b) The domains remain the same after retracting the electric field, showing the retention behavior of the domains. (c) The domain configuration after applying the reversed electric field (-60kV cm^{-1}). The surface γ- and β- domains shrink. (d)-(f) Schematics of the domain configurations for (a)-(c), respectively.

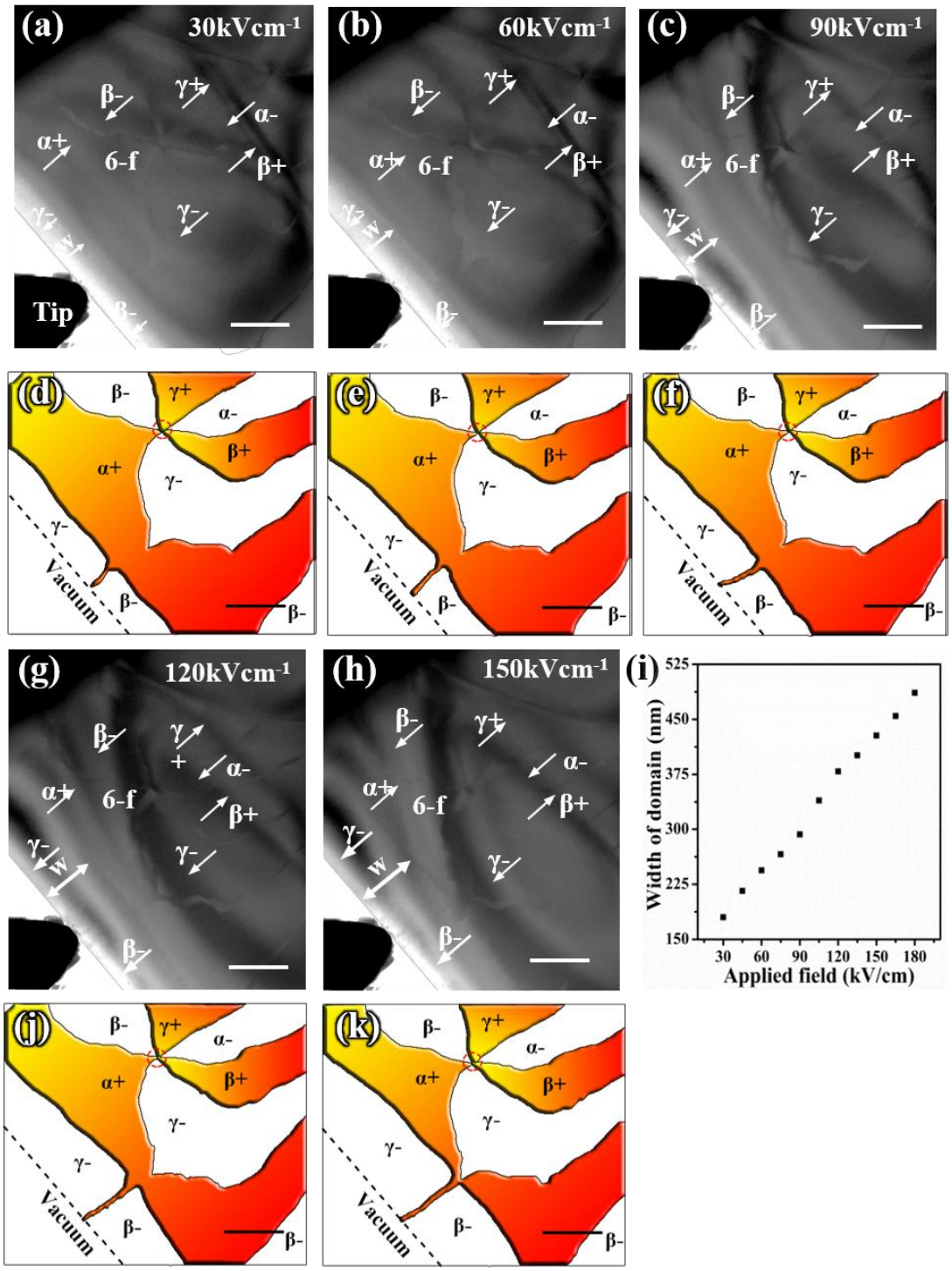

Figure 4. Domain evolution under different applied bias. (a)-(c) (g) (h) The domain configurations at different external bias. The domain switching only happens at the surface area and width of switched domains is denoted as "w". The polarization direction and phase of each domain are illustrated. All the scale bars represent 400 nm. (i) The linear-like relationship between the width of domain and the external applied field. (d)-(f) The

schematics of the domain configurations for (a)-(c), resepectivley. (j) (k) The schematics of the domain configurations for (g) and (h), respectively.

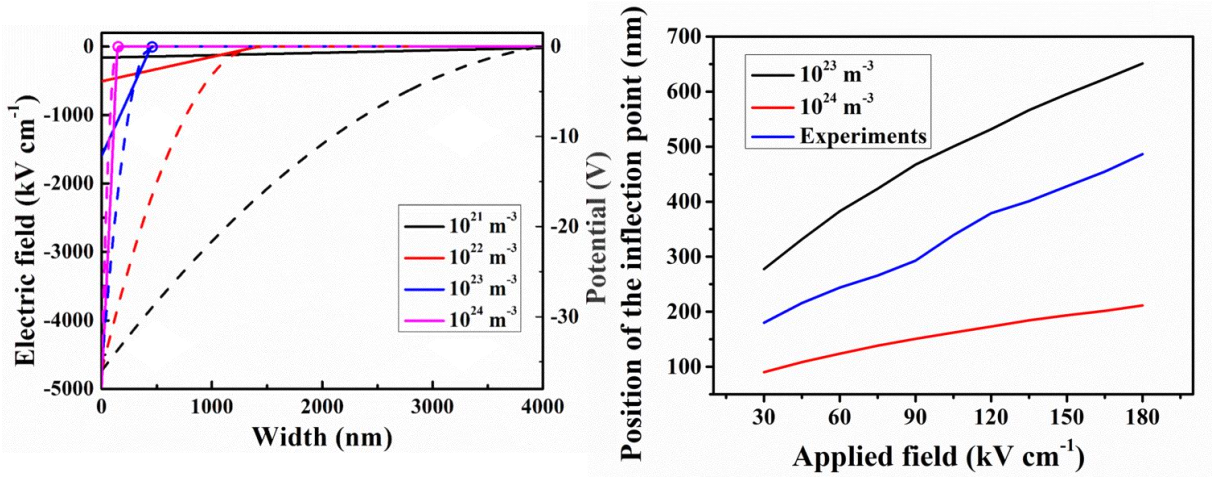

Figure 5. Numerical simulations of the distribution of electric fields in $YMnO_3$ sample. (a) Spatial dependence of the electric field strength and electric potential in $YMnO_3$ sample for different carrier densities under 90 kV cm^{-1} external bias. The solid lines are the simulated electric field strength, while the dashed lines are the corresponding electric potential. The inflection points of carrier densities of 10^{23} m^{-3} and 10^{24} m^{-3} (pink and blue lines) are circled. Sharp transition of electric field is expected when the concentration of charge carriers is high. The width of the sample is defined in Figure 2(b). (b) The relationship between positions of inflection points and external applied electric fields for two carrier concentrations (10^{23} m^{-3} and 10^{24} m^{-3}). The experimental result is replotted here as blue line.

Table of contents entry

We reveal the effects of trace oxygen vacancies on switching behaviors in multiferroic $YMnO_3$ single crystal using *in-situ* biasing and Landau based numerical calculations. The domain switching only occurs near the topmost surface area under different electric fields, which can be attributed to the electric field redistribution induced by the oxygen vacancies.

Keywords: *in-situ* biasing, domain switching, hexagonal manganites, oxygen vacancies

Shaobo Cheng, Qingping Meng, Myung-Geun Han, Shiqing Deng, Xing Li, Qinghua Zhang, Guotai Tan, Gianluigi A. Botton, Yimei Zhu**

Revealing the effects of trace oxygen vacancies on improper ferroelectric manganite with *in-situ* biasing

ToC figure

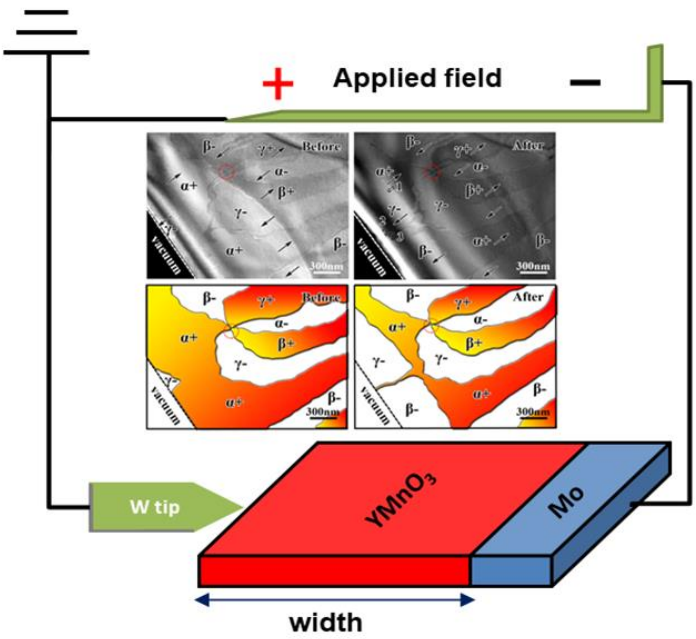

Supporting Information

Revealing the effects of trace oxygen vacancies on improper ferroelectric manganite with *in-situ* biasing

Shaobo Cheng, Qingping Meng, Myung-Geun Han, Shiqing Deng, Xing Li, Qinghua Zhang, Guotai Tan, Gianluigi A. Botton, Yimei Zhu**

Prof. Yimei Zhu, Dr. Shaobo Cheng, Dr. Qingping Meng, Dr. Myung-Geun Han
Condensed Matter Physics and Materials Science, Brookhaven National Laboratory, Upton, NY 11973, USA
*E-mail: zhu@bnl.gov
chengs36@mcmaster.ca

Prof. Gianluigi A. Botton, Dr. Shaobo Cheng
Department of Materials Science and Engineering, McMaster University, Hamilton, Ontario, L8S 4L7, Canada

Mr. Shiqing Deng
School of Materials Science and Engineering, Tsinghua University, Beijing 100084, China

Dr. Xing Li
Key Laboratory of Materials Physics of Ministry of Education, Department of Physics and Engineering, Zhengzhou University, Zhengzhou 450052, China

Dr. Qinghua Zhang
Beijing National Laboratory for Condensed Matter Physics Institute of Physics, Chinese Academy of Sciences, Beijing 100190, China

Prof. Guotai Tan
Department of Physics, Beijing Normal University, Beijing 100875, China

Keywords: *in-situ* biasing, domain switching, hexagonal manganites, oxygen vacancies

1. The calculation details

The space charge in the sample density is given by: [1]

$$\rho(x) = N_0(x) - n(x) \quad \text{(S1)}$$

where $N_0(x)$ is twice the concentration of oxygen vacancies, and $n(x)$ is the electron concentration which can be approximated by:

$$n(x) = n_0 \exp[\frac{e\phi(x)}{k_B T}] \quad \text{(S2)}$$

where $\phi(x)$ is the electric potential, k_B is the Boltzmann's constant, T is the temperature, and n_0 is the electron concentration. In our simulation, we assume $n_0 = N_0$ in the bulk material. The relative dielectric constant is defined as:

$$\varepsilon_r = 1 + \frac{1}{\varepsilon_0}\frac{\partial P}{\partial E} \quad \text{(S3)}$$

where ε_0, P, and E are the permittivity of free space, the polarization, and the electric field inside the sample, respectively.

Using the Landau theory, the free energy density expansion in multiferroic $YMnO_3$ can be represented in the following form: [2]

$$f = \frac{a}{2}Q^2 + \frac{b}{4}Q^4 + \frac{c + c'\cos(6\theta)}{6}Q^6 - gQ^3P\cos(3\theta) + \frac{g'}{2}Q^2P^2 + \frac{a_P}{2}P^2 \quad \text{(S4)}$$

The numerical values of the parameters *a*, *b* and so on in equation (S4) are taken from Ref. [2]. For simplicity, only $\theta = 0$ domain is considered. The order parameter Q in equation (S4) is obtained by minimizing the free energy density:

$$aQ + bQ^3 + (c + c')Q^5 - 3gQ^2P + g'QP^2 = 0 \quad \text{(S5)}$$

Based on the Landau expansion, we obtain the relationship between the electric field $E(x)$ and the polarization *P(x)* as following:

$$E(x) = -gQ^3 + g'Q^2P + a_P P \quad \text{(S6)}$$

Since the electric field is spatially varied, Q, P, and the relative dielectric constant are presumably to be the functions of the positions. So the relative dielectric constant can be expressed as:

$$\varepsilon_r(x) = 1 + \frac{1}{\varepsilon_0(a_P + g'Q^2)} \tag{S7}$$

Using Gauss's law, we obtain

$$\frac{\partial}{\partial x}(\varepsilon_r(x)\frac{\partial\phi(x)}{\partial x}) = -\frac{q\rho(x)}{\varepsilon_0} \tag{S8}$$

Combining equations (S5)~(S8), we can numerically solve the electric potential, dielectric constants, *Q* and *P* in the sample.

2. Figures and captions

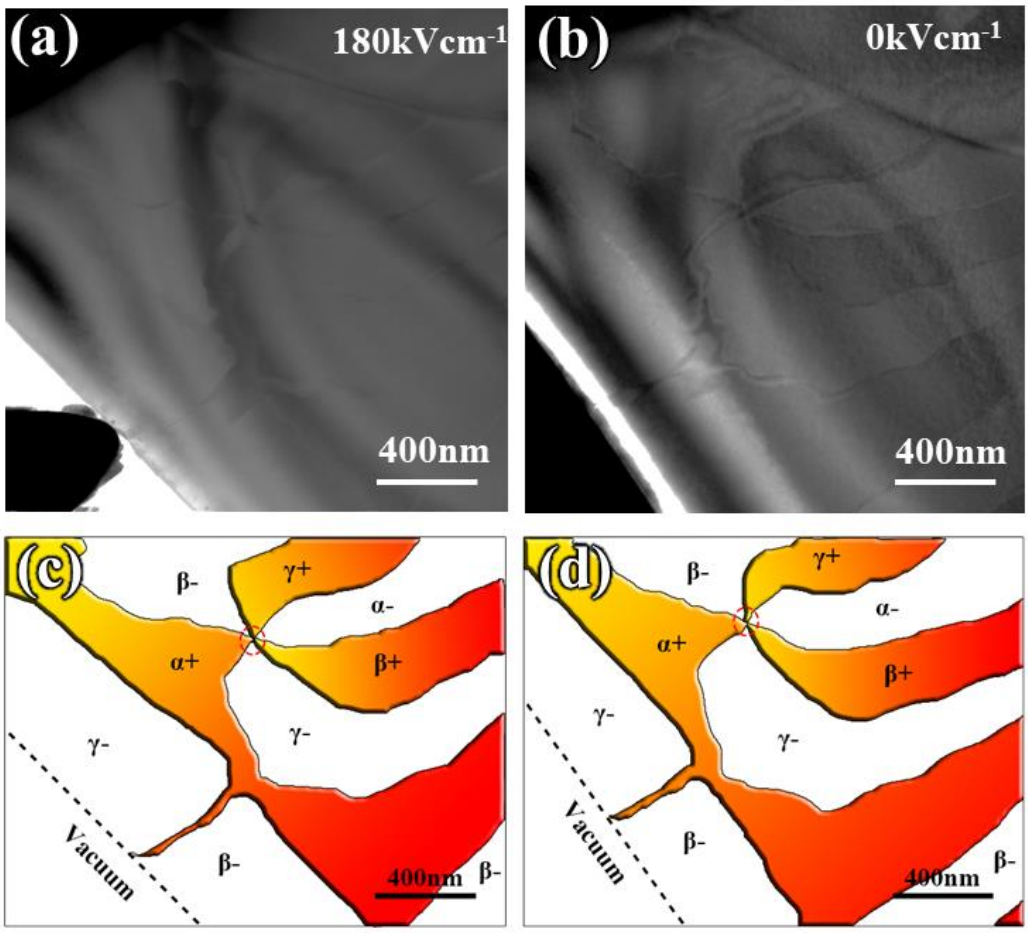

Figure S1. Retention behaviors for the switched domains. (a) TEM image acquired in the *in-situ* experiment at 180 kV cm^{-1} biasing. The W tip can be observed at the bottom left corner. (b) TEM image acquired after *in-situ* experiment. The W tip has been retracted. The domain

configuration stays the same. (c)(d) Schematic diagrams for the domain configurations in (a) and (b), respectively.

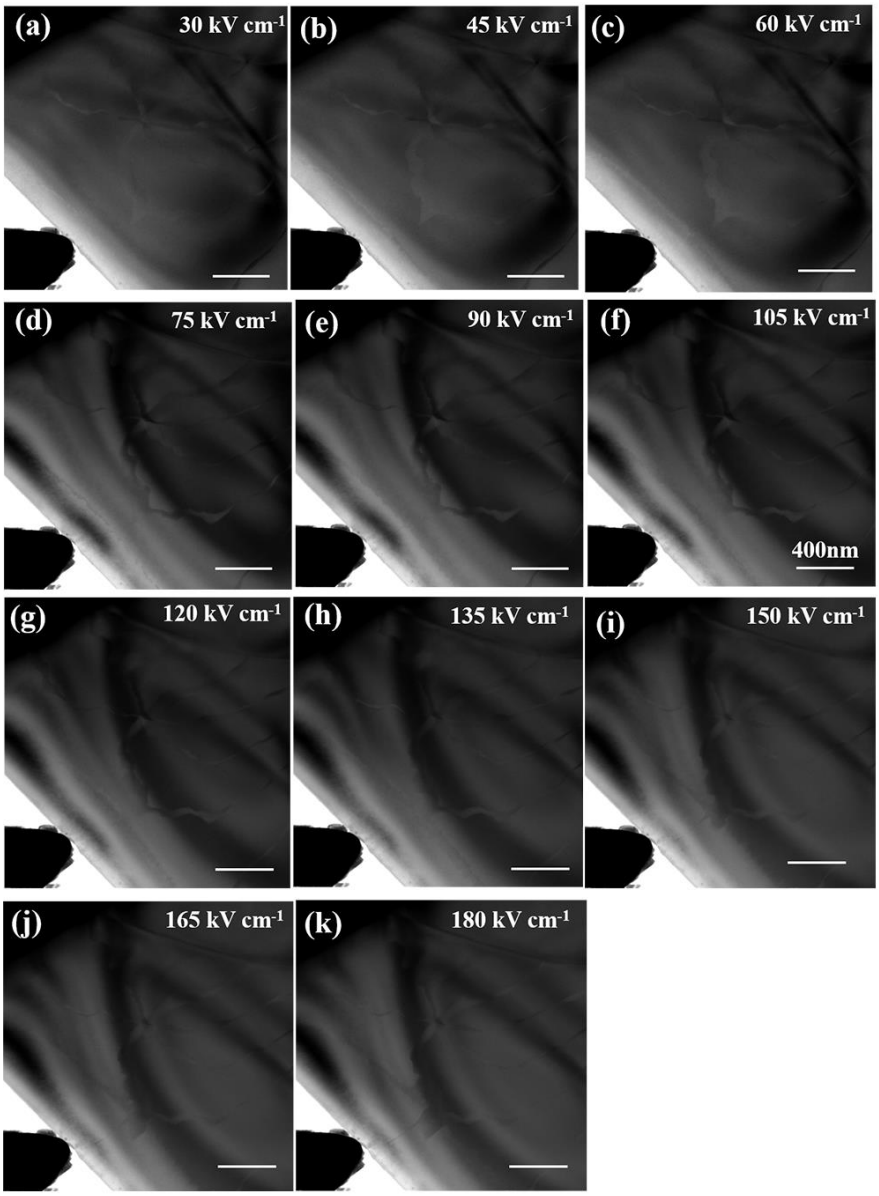

Figure S2. Sequential TEM images showing the movement of domain fronts at different electric fields (from 30 kV cm^{-1} to 180 kV cm^{-1}). The width of domain front increases linearly with the external fields strength.

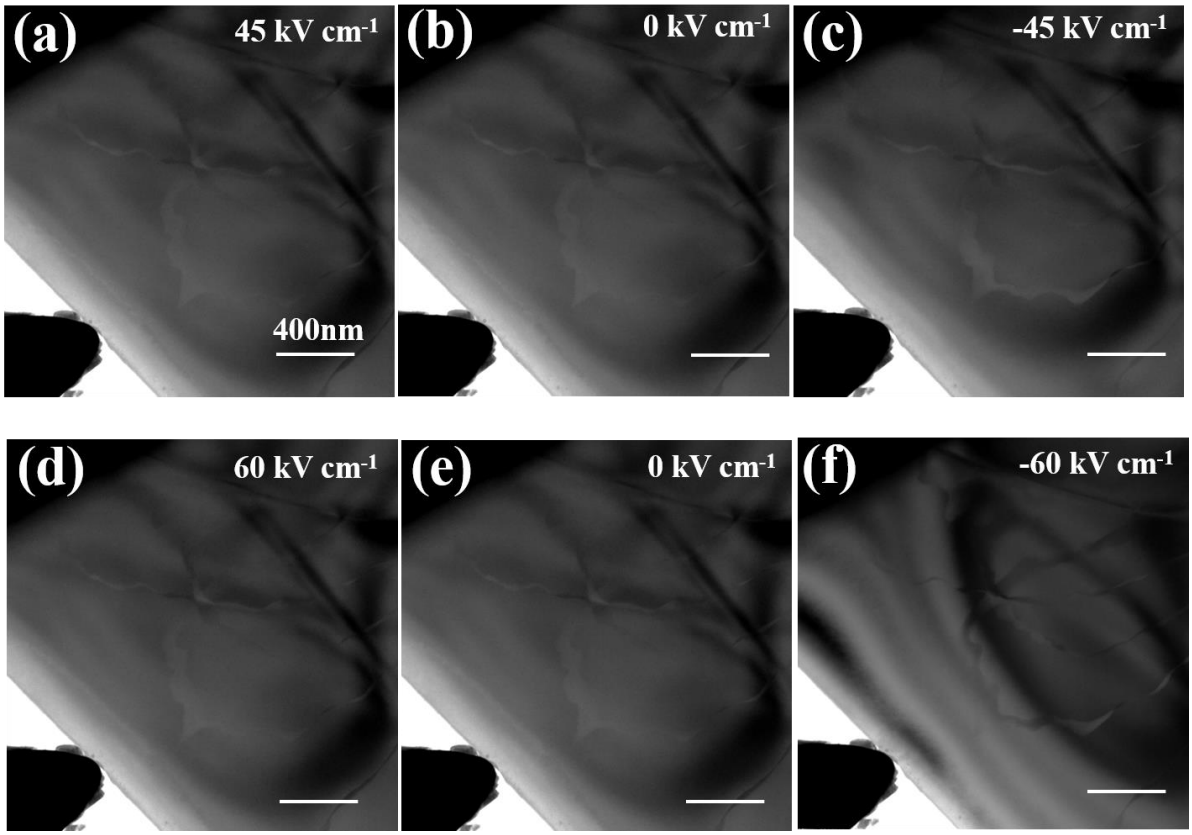

Figure S3. Switching dynamics of domains at the surface area under 45 kV cm^{-1} and 60 kV cm^{-1}. (a) The domain front is created under 45 kV cm^{-1} external bias, which corresponds to the "write" process in multiferroic device. (b) The domain front remains when the external bias is zero. (c) The domain front disappears when a reverse electric field is applied, corresponding to the "erase" process. (d)-(f) Another "write" and "erase" circle under 60 kV cm^{-1}.

References:

[1] J. Zhang, M. H. Tang, J. He, *Appl. Phys. Lett.* **2010**, 96, 122905

[2] S. Artyukhin, K. T. Delaney, N. A. Spaldin, and M. Mostovoy. *Nat. Mater*.**2013**, 13, 42